Electronic Supplementary Materials

For https://doi.org/10.1631/jzus.A2400038

Effect of mesoporous FA-SiO_2 extracted from fly ash on the structural and photocatalytic properties of g-C_3N_4-based materials

Xianhua LI[1,2], Qingbo YU[1,3]

[1]*The First Hospital of Anhui University of Science & Technology, Anhui University of Science & Technology, Huainan 232001, China*

[2]*School of Mechatronic Engineering, Anhui University of Science & Technology, Huainan 232001, China*

[3]*School of Materials Science and Engineering, Anhui University of Science & Technology, Huainan 232001, China*

Section S1 Kinetic analysis of thermal decomposition

The reaction activation energy *E* was calculated by the *Flynn-Wall-Ozawa* (FWO) method with the following expression (1):

$$lg\ \beta = lg\left[\frac{AE}{RG(\alpha)}\right] - 0.4567\frac{E}{RT} - 2.314 \quad \text{(S1)}$$

In the expression: β represents as the heating rate; *E* is represents activation energy; α represents as the conversion rate; $G(\alpha)$ represents as the integral function of α; *A* represents the pre-exponential factor; *T* represents temperature; *R* represents the gas constant, with a value of 8.314 J/(K ·mol).

When the temperature *T* corresponding to the same conversion rate α at different heating rates β (10、15、20 ℃/min) is chosen, a scatter plot of *lgβ-1/T* is plotted and the curve is fitted using least squares to obtain a fitted curve, and the activation energy *E* is calculated from the slope of this fitted curve.

At a certain temperature, we can express the thermal decomposition process by

combining the order of time and conversion rate $\alpha(t)$ with the function of reactant concentration $f(\alpha)$ through a rate constant $k(T)$. The expression (2) is as follows:

$$\frac{d\alpha}{dt} = \left(\frac{1}{\beta}\right) k(T) f(\alpha) \tag{S2}$$

Since the relationship between the reaction rate constant and temperature follows the *Arrhenius* relation, in order to estimate the relationship between temperature and conversion rate *α*, the kinetic model is coupled with the *Arrhenius* relation to get the expression (3):

$$\frac{d\alpha}{dt} = \frac{A}{\beta} exp(-\frac{E}{RT}) f(\alpha) \tag{S3}$$

Reaction rate and conversion rate α there is a corresponding functional relationship between them and it can represent the reaction mechanism and its integral expression can be defined as:

$$G(\alpha) = \int_0^{\alpha} \frac{d\alpha}{f(\alpha)} \tag{S4}$$

Combine the expressions (3) and (4), it can be obtained:

$$G(\alpha) = \int_{T_0}^{T} \frac{A}{\beta} exp\left(-\frac{E}{RT}\right) dT \approx \int_0^{T} \frac{A}{\beta} \exp\left(-\frac{E}{RT}\right) dT = (\frac{AE}{\beta R}) P(u) \tag{S5}$$

Where $P(u)$ is expressed as the temperature integral, then $u = \frac{E}{RT}$. Using α = 0.5 as the reference point, the following expression is obtained:

$$\frac{P(u)}{P(0.5)} = \frac{G(\alpha)}{G(0.5)} \tag{S6}$$

In order to calculate $P(u)$, an approximate expression is introduced using mathematical approximation:

$$P(u) = \frac{e^{-u}}{u(1.00198882u+1.87391198)} \tag{S7}$$

In expression (6), $\frac{P(u)}{P(0.5)}$ is the experimental data and $\frac{G(\alpha)}{G(0.5)}$ is the theoretical function. The activation energy *E* value can be substituted into $P(u)$ and $P(0.5)$, and then the corresponding value of conversion α can be obtained, and the scatter plot can be drawn. Compare whether all the points in the scatter plot fall on or near the theoretical curve. If it falls near several curves, the dynamics model that is closest to the theoretical value is determined by the standard deviation formula. The smaller the value of Δk, the more consistent the mechanism function. The expression to calculate

the standard deviation is as follows:

$$\Delta k = \sqrt{\sum_i^m \left[\frac{P(u_i)}{P(u_{0.5})} - \frac{G_k(\alpha_i)}{G_k(\alpha_{0.5})}\right] / (m-1)} \quad \text{(S8)}$$

Where, m represents the number of data points, and k represents the sequence number of the reaction mechanism function. When the value of Δk is the smallest, this function is the most appropriate mechanism function.

Substitute the integral expression of the resulting mechanism function into expression (5), it can be obtained that:

$$ln(\frac{E}{\beta R}) + lnP(u) = -lnA + lnG(\alpha) \quad \text{(S9)}$$

When the rate of warming β is determined, a scatter plot is plotted against $lnG(\alpha)$ by $[ln\left(\frac{E}{\beta R}\right) + lnP(u)]$ and the resulting data points are then fitted to a straight line, and the value of the finger front factor A is obtained by the intercept of the line.

Section S2 Characterization

The crystal structure of the sample was analyzed using an XRD-6000 X-ray diffractometer (XRD), and the scanning angle range and speed are 5 °- 80 °and 5 °/min, respectively. Fourier transform infrared spectrometer (FT-IR) with Nicolet 380 was used to analyze the characteristic functional groups of the samples. The morphological characteristics of the samples were analyzed using a FlexSEM1000 scanning electron microscope (SEM). The chemical state of the samples was determined using X-ray photoelectron spectroscopy (XPS) of type ESCALAB 250Xi, and binding energy was calibrated concerning the C 1s peak (284.8 eV). The thermal polymerization process of the precursor synthetic carbon nitride was analyzed using a STA449F5 thermal gravimetric analyzer. The samples were placed in corundum crucibles and calcined from 25 ℃ to 800 ℃ at ramp rates of 10 ℃/min, 15 ℃ /min , and 20 ℃/min, respectively, and subjected to TG analysis under an N_2 atmosphere. The simulated pollutant methylene blue (MB) was degraded using the CEL-HXF300 xenon lamp light source system, and its absorbance was measured using a UV-1800 ultraviolet-visible spectrophotometer to evaluate the photocatalytic performance of the sample. The Lambda 950 ultraviolet-visible spectrometer was

used to analyze the diffuse reflectance spectrum of the sample and determine its optical absorption performance. The photoluminescence spectrum (PL) of the sample was measured using the FLS980 fluorescence spectrometer, with the excitation wavelength set at 438 nm.

Section S3 Photocatalytic performance test

The photocatalytic performance of the samples was tested by simulating the efficiency of visible light degradation of methylene blue (MB), and the CEL-HXF300 xenon lamp light source system was used to simulate visible light, and the light source was a 300 W xenon lamp equipped with a 420 nm ultraviolet cut-off filter. Firstly, 40 mg of the photocatalyst was dispersed in 100 mL of methylene blue solution with a mass concentration of 20 mg/L and stirred in the dark for 1 h before irradiation to achieve adsorption-desorption equilibrium. After the irradiation started, 4 mL of solution was taken every 10 min and centrifuged to obtain the supernatant, and the absorbance was measured and recorded at the wavelength of 664 nm by UV-1800 UV-visible spectrophotometer.

Section S4 Photoelectrochemical performance test

Using a three-electrode system, the transient photocurrent response curve and the electrochemical impedance spectroscopy (EIS) of the sample were measured by using the CHI660E electrochemical system. A 300 W xenon lamp fitted with a 420 nm UV cut-off filter was used as the light source and the intensity of incident visible light was measured as 1.2 mW/cm^2 by FZ-A irradiation meter. A mixed solution was prepared by mixing 5 mg of sample and 5 μL Nafion solution with 5 mL of anhydrous ethanol. The mixture was sonicated to form a homogeneous suspension, and 20 μL of the suspension was dropped onto the surface of a conductive glass (1*2 cm), dried naturally and then made into a working electrode, with an Ag/AgCl electrode as the reference electrode, a platinum wire as the counter electrode and Na_2SO_4 (0.2 M) aqueous solution as the electrolyte.

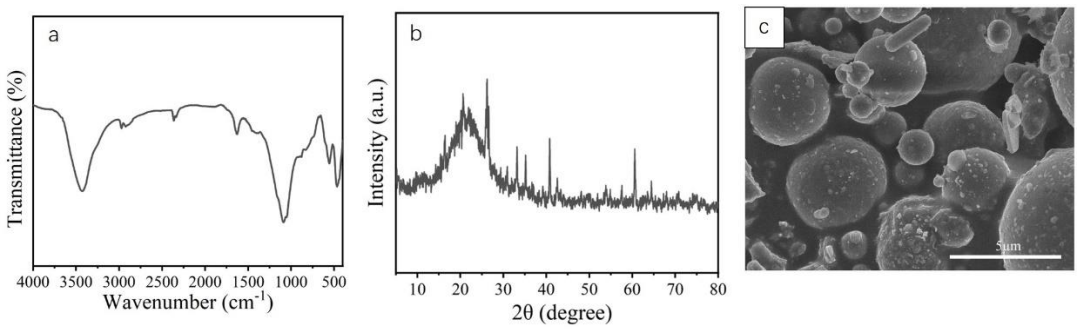

Fig. S1 (a) FT-IR spectra, (b) XRD spectra and (c) SEM of fly ash

Fig. S2a illustrates the IR spectra of silicon dioxide prepared by two different methods. For TEOS-SiO_2, the absorption peak at 468 cm^{-1} is attributed to the bending vibration of Si-O-Si. The absorption peaks at 798 cm^{-1} and 1091 cm^{-1} correspond to the symmetric stretching vibration peak and asymmetric stretching vibration peak of Si-O-Si, respectively, which are characteristic absorption peaks of SiO_2.The absorption peak at 959 cm^{-1} is attributed to the bending vibration of Si-OH. The peak at 1640 cm^{-1} corresponds to the bending vibration peak of adsorbed water. The strong absorption peak at 3435 cm^{-1} is related to the -OH stretching vibration. The peak intensity and position of FA-SiO_2 remain basically the same compared to TEOS-SiO_2. The above results indicate that SiO_2 was successfully prepared.

Fig. S2b shows the XRD spectra of silicon dioxide prepared by two different methods, it can be seen that TEOS-SiO_2 and FA-SiO_2 have a broader peak between 20-30 °, which is an amorphous diffraction peak, and no sharp crystalline diffraction peaks were observed, so TEOS-SiO_2 and FA-SiO_2 are amorphous silicon dioxide.

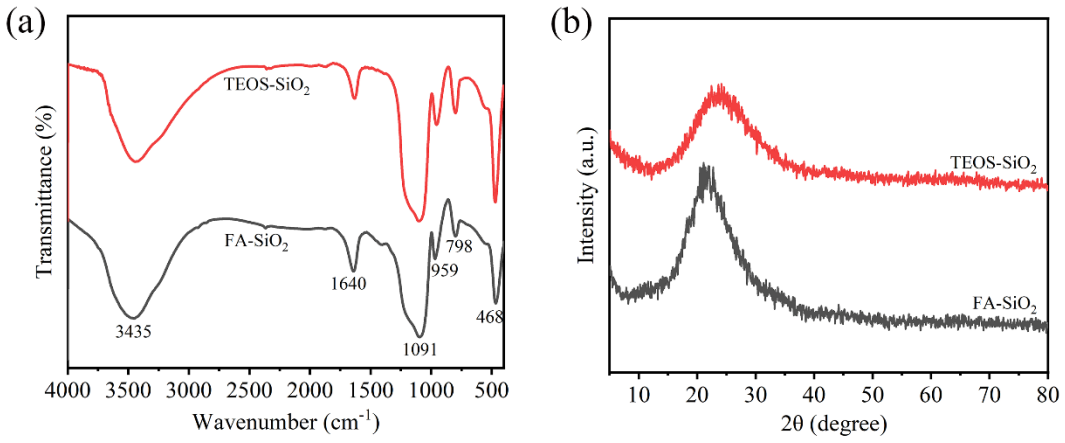

Fig. S2 (a) FT-IR spectra and (b) XRD spectra of TEOS-SiO_2 and FA-SiO_2

Fig. S3 shows the SEM images of TEOS-SiO_2 and FA-SiO_2. From Figure S3a, it can be seen that TEOS-SiO_2 presents a spherical shape with a uniform and smooth surface and no obvious holes, and the particle size is uniform. FA-SiO_2 exhibits a blocky structure made up of a combination of fine particles (Figure S3b).

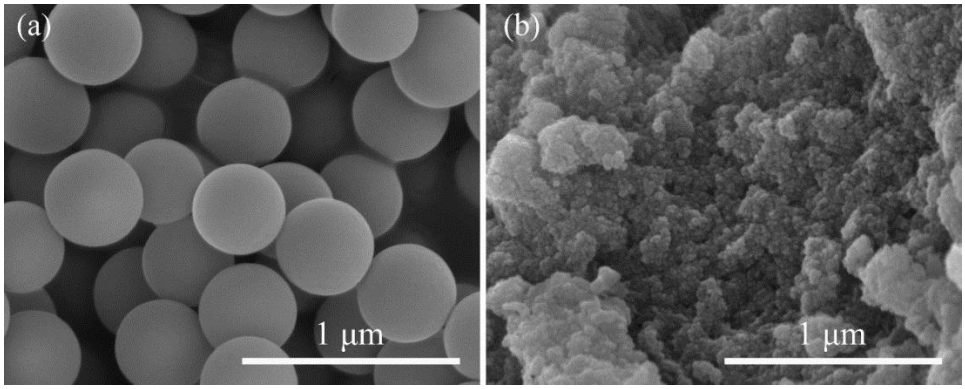

Fig. S3 SEM of (a)TEOS-SiO_2 and (b)FA-SiO_2

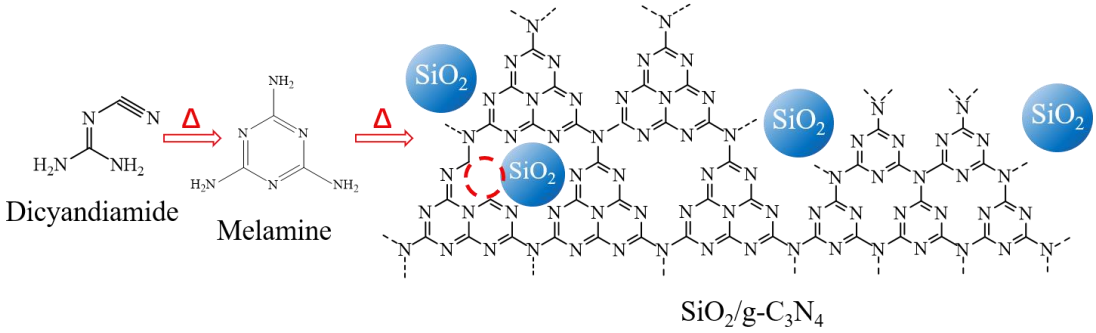

Fig. S4 The synthesis pathway of the SiO_2 and g-C_3N_4 composites

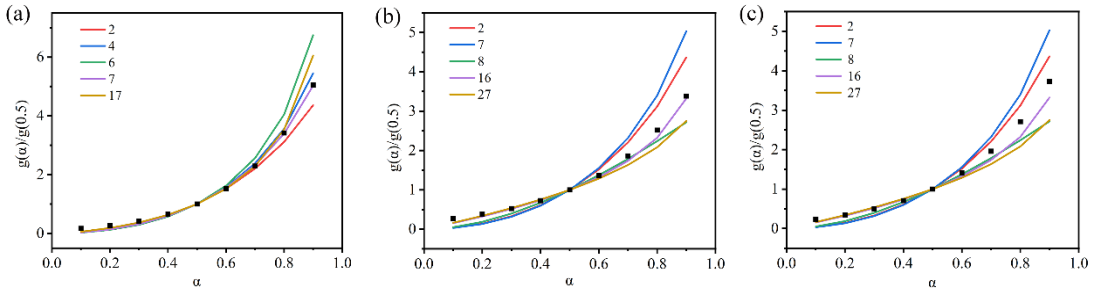

Fig. S5 Comparison of experimental data and standard curve of (a) DCDA, (b) TEOS-SiO_2/DCDA and (c) FA-SiO_2/DCDA

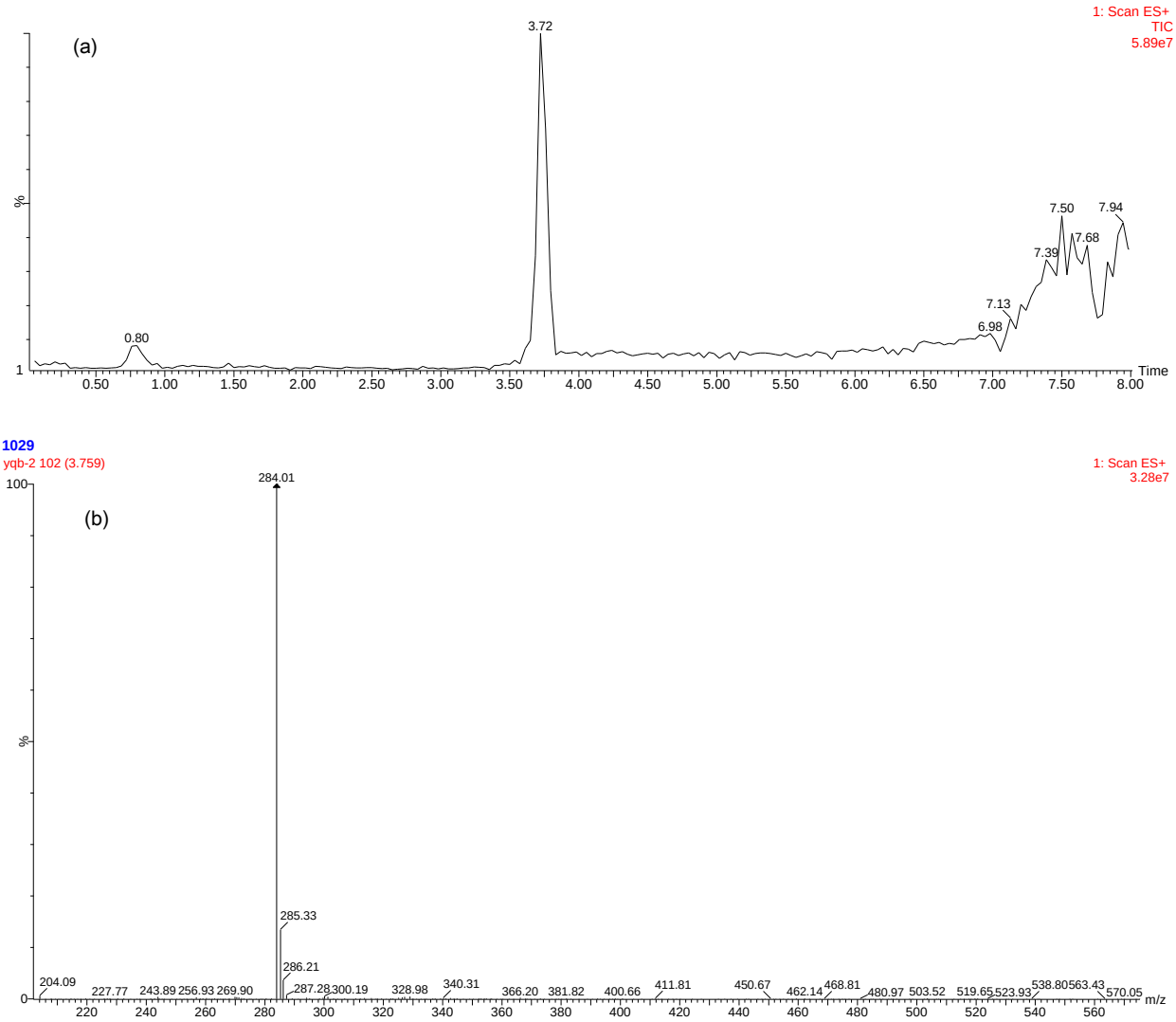

Fig. S6 (a) Liquid chromatogram and (b) Mass spectrum of M

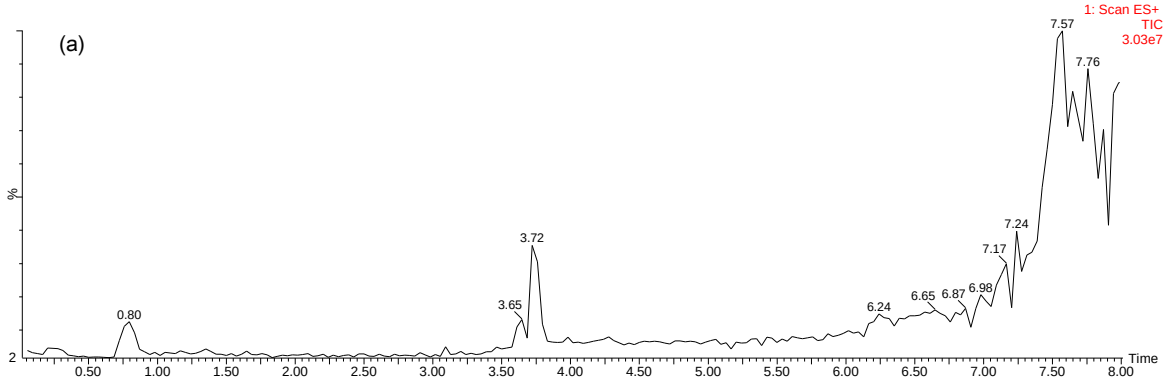

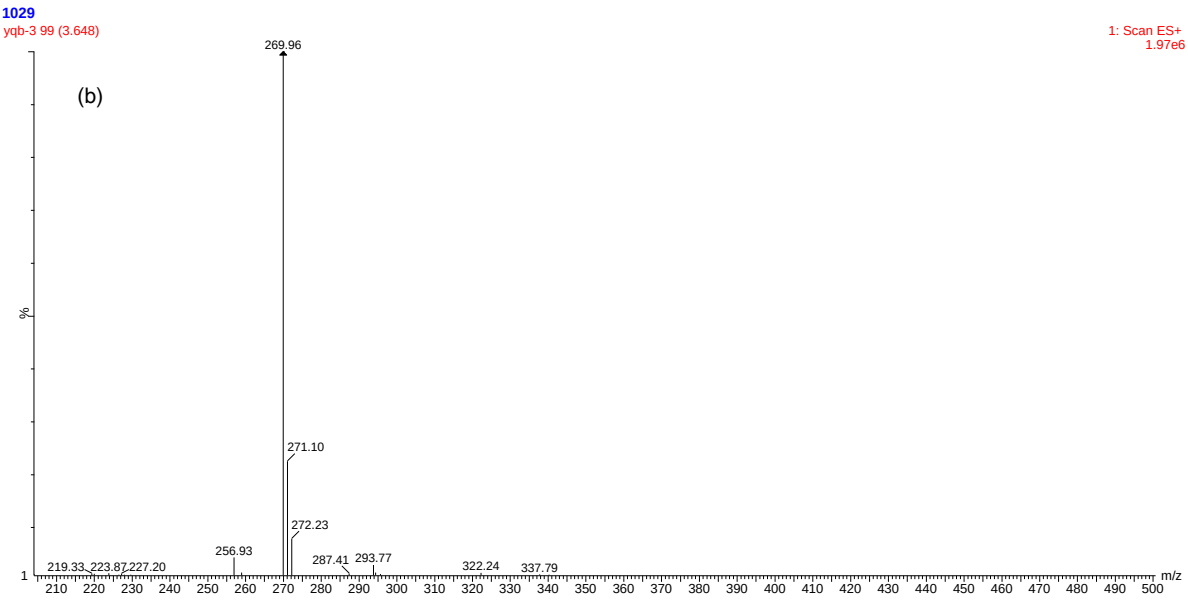

Fig. S7 (a) Liquid chromatogram and (b) Mass spectrum of MB after photocatalysis

Table S1 Contents of C, N, O and Si in g-C_3N_4, TEOS-SiO_2/g-C_3N_4 and FA-SiO_2/g-C_3N_4

Sample	C (%)	N (%)	O (%)	Si (%)
g-C_3N_4	31.98	59.85	8.17	/
TEOS-SiO_2/g-C_3N_4	14.93	15.07	49.23	20.76
FA-SiO_2/g-C_3N_4	20.78	26.26	34.90	18.06